Degradation of Electrographic Images Due to Surface Lateral Conduction*

I. Chen,† J. Mort, M. A. Machonkin, and J. R. Larson†

J. C. Wilson Center for Research and Technology, Xerox Corporation, Webster, New York 14580

The electrical conduction at the surface layer of a photoreceptor can cause degradation of electrostatic latent images in electrography. Previous studies of this phenomenon either have required a high-resolution probe for investigations of fine line patterns or have been limited by the probe size to investigations of broad line patterns. This report describes a coordinated theoretical and experimental study that enables the experiments made at conveniently low resolution and long times to predict the impact of lateral conduction in the regimes of high resolution and high process speed. The technique is illustrated with a layer of developed liquid toner on a photoreceptor, which has important implications in the electrical specification of toners for use in color-superimposing processes.

Journal of Imaging Science and Technology 40: 431–435 (1996)

Introduction

The quality of electrophotographic images depends critically on the ability of photoreceptors (PRs) to maintain the latent images, i.e., the imagewise charge distributions on the PR surface, in the period between exposure and development. In addition to "dark decay," which commonly refers to neutralization of the surface charges by charge generation and transport in the PR *bulk*, such latent images can also be degraded by lateral motion of charges in a thin layer near the PR *surface*. Such a thin semi-insulative (SI) layer can be formed on the PR surface by deterioration of the electronic properties ("fatigue") near the surface[1]; by contamination, e.g., from corona discharge[2, 3]; or by field effect band-bending.[4,5] Furthermore, in color electrophotography with the "color-superimposing process,"[6–8] a layer of previously developed color toners on the PR surface can be conductive enough to cause concern for the stability of latent images for the successive colors. This is particularly important when liquid toners are used,[9] because they are generally more conductive than dry toners. Liquid toners are composed of particles dispersed in a hydrocarbon fluid containing an ionic surfactant known as a *charge director* (CD), which forms inverse micelles in the hydrocarbon fluid. An interaction between the particles and the CD micelles charges the particles. This effect is used to enable the imagewise deposition of the particles on a charged latent image in electrostatic printing processes. The CD micelles also interact to self-ionize, forming both positive and negative species that increase the conductivity of the dispersion.[10,11]

As the demands for higher image resolution and process speeds grow, the investigations of the lateral conduction effects on the quality of thin line images (<50 μm wide) in short time periods (<0.1 s) of practical interest become experimentally very difficult. This report describes a coordinated theoretical and experimental study that overcomes this difficulty by enabling experiments made at conveniently low resolutions and long times to predict the impact of lateral conduction for high resolution and high process speed regimes of interest. The experimental technique and illustrative results obtained with developed liquid toners as the SI layer are described in the next section. This is followed by the theoretical analysis and numerical examples, which provide the insights for the extrapolation of macroscopic observations to microscopic phenomena. It is demonstrated that the technique can be used to evaluate efficiently and economically the applicability of a particular liquid toner for the color-superimposing processes.

Experimental Method and Results

The lateral conduction effect is investigated with samples consisting of a layer of developed liquid toners on an organic photoreceptor (essentially perfectly insulating in the dark), as shown schematically in Fig. 1. The SI toner layers are prepared from liquid toners of various conductivities by increasing the solid resin content from 2 to about 20%. The details of preparation and characteristics of the starting liquid toners can be found in Refs. 10, 11, and 12. The preparation of concentrated films is achieved by two methods. The first is simply by centrifuging a lower solid content liquid toner and reconstituting to the desired solid content. This is then drawbar coated onto the PR. In the

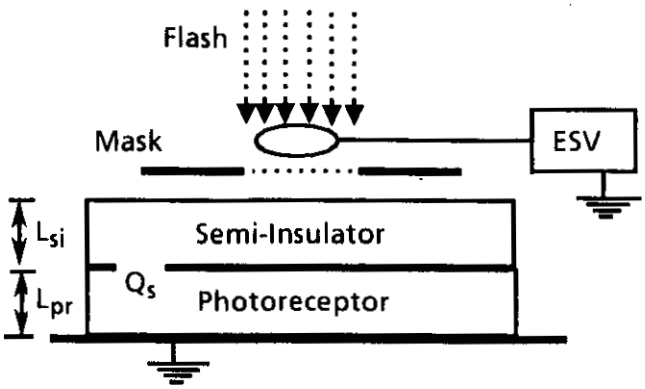

Figure 1. Schematic of sample structure and experimental setup.

Original manuscript received March 14, 1996. Revised July 16, 1996.

* Presented in part at IS&T's 12th International Conference on Digital Printing Technologies, October 27-November 1, 1996, San Antonio, Texas.

† IS&T Member

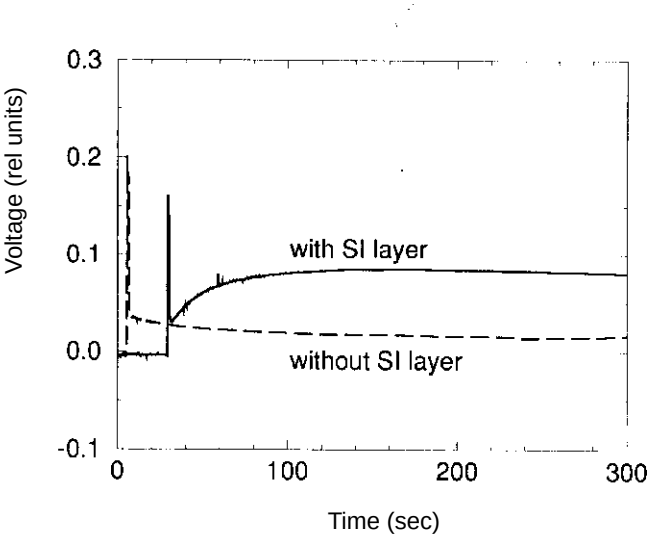

Figure 2. Surface voltage as a function of time during charging, exposure, and recovery by lateral conduction, for samples with and without developed liquid toner layer.

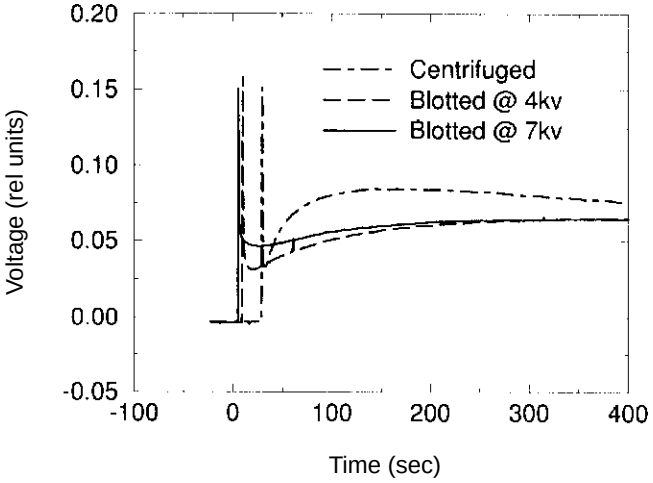

Figure 3. Surface voltage as a function of time during charging, exposure, and recovery by lateral conduction, for samples prepared by centrifuge and by bias-blotting.

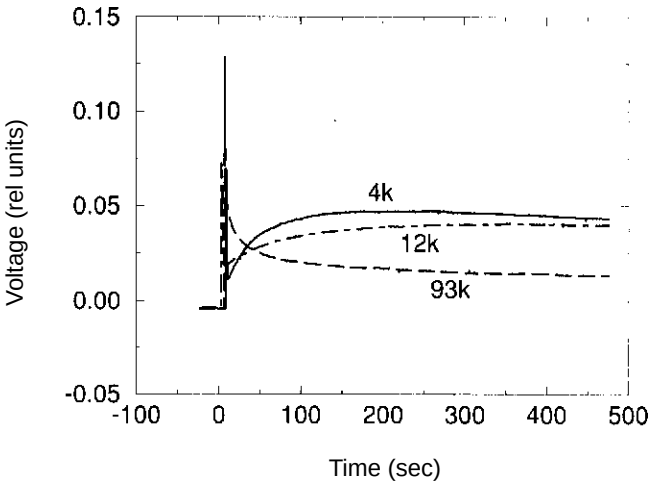

Figure 4. Surface voltage as a function of time during charging, exposure, and recovery by lateral conduction, for samples prepared from liquid toners containing charge director surfactants of different molecular weights (4000, 12,000 and 93,000).

second method, which is more closely related to the actual development, an electrical bias is applied to a layer of liquid toner on the PR, thereby moving the charged solid particles toward one side and the smaller sized counter ions to the other. The counter ions are then blotted away with the liquid. The films have a thickness from 10 to 50 μm and an area of ~7.5cm^2.

With the PR grounded, the composite layer is first corona charged uniformly, typically to several hundred volts. Then a circular area defined by a mask with a 6-mm-diameter opening is exposed with a 30-ms flash of white light, which almost completely discharges the exposed area. The surface voltage of the circular area is continuously monitored, typically over several hundred seconds, with a shielded loop probe (4 mm in diameter) connected to a Keithley electrometer coupled with a Nicolet digital storage oscilloscope.

A representative data plot is shown in Fig. 2. The two curves in this figure are obtained with and without the overlying SI toner layer. The fast photoinduced decay of the surface voltage (combined with the initiation of signal recording) appears as a spike at the exposure time. Without the SI layer, the surface voltage remains low after the discharge. In the sample with the SI layer, the lateral conduction effect manifests itself by a recovery in surface voltage after the initial sharp discharge. The voltage recovery reduces the electrostatic contrast between the exposed and the unexposed areas.

Figure 3 shows data that compare the effects in SI layers produced by centrifuge and bias-blotting methods. It is apparent that the effect is smaller in a bias-blotted layer. Because the toner particles in 20% solid film are considered essentially immobile, the lateral conduction is mainly due to the motion of the counter ions, which is also consistent with a field-controlled extraction of counter ions during the bias-blotting process.

The results obtained with SI layers prepared from different source liquid toners are shown in Fig. 4. The source liquid toners are prepared with three charge-director (CD) surfactants of different molecular weights (4000, 12,000 and 93,000).[12] Whereas the voltage recovery decreases in going from samples containing the lowest molecular weight CD to that with the medium molecular weight CD, no recovery is detectable in the sample with the highest molecular weight CD, even with an increased concentration of 0.2 wt% or films as thick as 50 μm. Based on the theoretical analysis presented in the next section, this result can only be rationalized if the conductivities of the SI layers differ by at least an order of magnitude. I–V measurements on the 20% solid film have yielded a conductivity of about 1 pS/cm for the least conductive layer. The low conductivity of the sample with the highest molecular weight CD is caused by the increase in micelle size, which in turn reduces the density and mobility of the charged micelles.

In addition, the following features associated with this voltage recovery have been observed: (1) After a few hours of air-drying, the effect disappears on samples that have shown voltage recovery. (2) No effect is detectable with SI layers prepared with liquid toners containing lower than 0.02 wt% of CD surfactants. (3) For the layers prepared with liquid toners containing higher CD concentration (>0.05 wt%), the effect is seen to increase progressively because of the associated larger conductivities in the source liquid. (4) For a given source liquid, the effect increases with the layer thickness.

Theoretical Analysis

Consider an SI layer of thickness L_{SI} on top of the grounded PR, as shown in Fig. 1. After charging the PR to a uniform voltage of V_o, the imagewise exposure creates a latent image, which can be represented by a surface charge density distribution Q_s located at the PR surface. For an exposure with a circular beam that creates a Gaussian surface charge distribution, Q_s at a distance r from the beam center can be written as

$$Q_s(r) = C_{PR}V_o[1 - \exp(-2r^2/R^2)], \quad (1)$$

where R is the $1/e^2$ radius of the Gaussian, and C_{PR} is the capacitance of the PR.

The surface voltage above the composite layer, $V(r,t)$, as a function of the radial coordinate r and time t, is related to the local charge densities, $Q_s(r)$ at the interface and $Q(r,t)$, the charge density per area in the SI layer at time t, as

$$V(r,t) = [Q_s(r) + Q(r,t)(1 + C_{PR}/2C_{SI})]/C_{PR}, \quad (2)$$

where C_{SI} is the capacitance of the SI layer. It is assumed that the charge $Q(r,t)$ is uniformly distributed across the SI layer thickness.

Up to the moment of latent image formation, $t = 0$, the SI layer is charge neutral. Hence, $Q(r,0)$ is zero everywhere, and from Eq. 2, the voltage distribution $V(r,0)$ has the same form as the interface charge density distribution $Q_s(r)$. The lateral field arising from this voltage distribution sets the charge carriers in the SI layer into motion, which can be described by the continuity equations for the positive and negative charge carrier densities (per area), $Q_p(r,t)$ and $Q_n(r,t)$:

$$\partial Q_p/\partial t = -\partial(\mu Q_p E)/\partial r, \quad (3)$$

$$\partial Q_n/\partial t = \partial(\mu Q_n E)/\partial r, \quad (4)$$

where μ is the charge mobility (assumed to be the same for positive and negative charges) and E is the local field strength, given by

$$E(r,t) = -\partial V(r,t)/\partial r. \quad (5)$$

The interface charge distribution $Q_s(r)$ is assumed to remain constant with time. The deviations of Q_p and Q_n from the initial, equilibrium value $\pm Q_o$ result in a net charge in the SI layer, $Q(r,t)$, as

$$Q(r,t) = Q_p(r,t) + Q_n(r,t), \quad (6)$$

which, in turn, modifies the voltage distribution $V(r,t)$, according to Eq. 2. In the exposed area ($r \le R$), the voltage "recovers" from the initial discharged value toward the preexposure value V_o, leading to a loss in the voltage contrast between the exposed and unexposed areas. The neglect of sample thickness dimension in the above treatment could be a poor approximation when the lateral dimension (e.g., R) is small compared with the sample thickness (~20 μm).

The above set of equations can be solved numerically for $V(r,t)$ as a function of time and position. Figure 5 shows an example of the surface voltage $V(r,t)$ as a function of distance r from the beam center at various times t after exposure for a given SI sample specified by the Q_o and C_{SI} values.

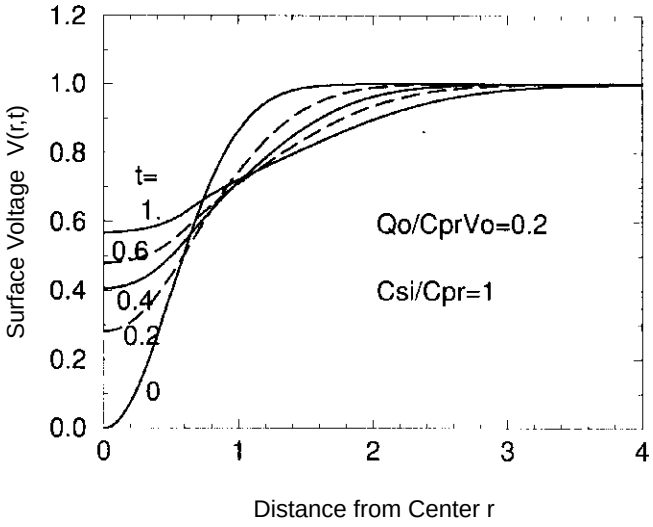

Figure 5. Calculated surface voltage distributions $V(r,t)$ at different times t, in units of t_o defined by Eq. 7. The voltage is in units of the preexposure value V_o, and the distance in units of the $1/e^2$ radius R of the Gaussian beam.

In this and the following figures, the numerical results are presented with the beam radius R, the charge mobility μ, the initial (undischarged area) voltage V_o, and the PR capacitance C_{PR} as the units for these basic quantities. The units for other quantities are derived from these four basic units. For example, the time t_o for the charge to move a distance R at a field V_o/R can be chosen as the units for time,

$$t_o \equiv R^2/\mu V_o. \quad (7)$$

Similarly, the charge density per unit area can be measured in units of $C_{PR}V_o$. With this system of units, the solutions of the above equations are determined by only two parameters, the initial equilibrium charge density Q_o in units of $C_{PR}V_o$, and the SI layer capacitance C_{SI} in units of C_{PR}. The beam radius R is implicit in the time scale. In other words, for a given SI layer, specified by given values of $Q_o/C_{PR}V_o$ and C_{SI}/C_{PR}, the fractional recovery of the surface voltage (shown in the figures) is independent of the beam radius (or the "dot size"), but the time to reach that extent of recovery varies quadratically with the radius. This relationship will be clear from the following numerical examples.

This observation allows the experiments, made at conveniently large dot sizes and long times, to predict the impact of lateral conduction in the regimes of high resolution and high process speeds of technological interest, not easily accessible.

Returning to Fig. 5, it can be seen that the voltage within the exposed area ($r \le 1$) recovers with time at the expense of the unexposed area ($r > 1$). The dot size broadens and the voltage contrast decreases as much as 50% in a time of the order of one time unit t_o. With typical values of V_o = 500 V, $\mu = 5 \times 10^{-6}$ cm²/Vs, and R = 25 μm (i.e., 500 dots per inch), the unit of time is t_o = 2.5 ms, which is shorter than the time period between exposure and development in general. On the other hand, for detection of this effect by the electrostatic voltmeter, the smallest beam radius is limited by the size of the voltage probe and is of the order of 2.5 mm. In this case, the time unit becomes t_o = 25 s, which is more convenient for laboratory observations of the effect. According to the above theoretical analysis, the

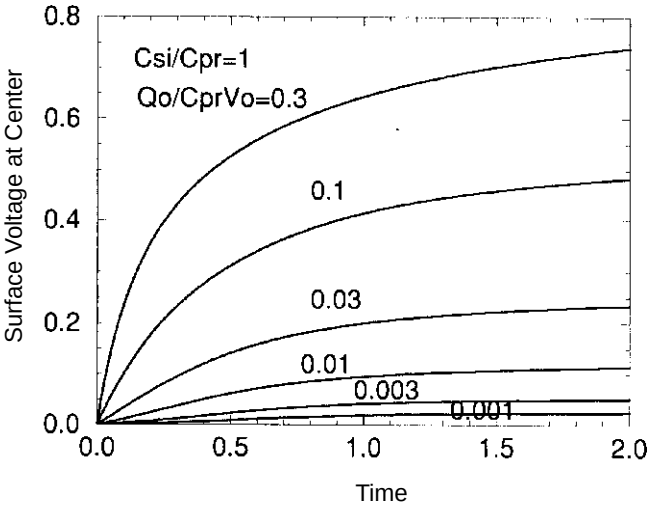

Figure 6. Calculated surface voltage at beam center as a function of time, for SI layers of various charge densities Q_o. The units are t_o for time, V_o for voltage, and $C_{PR}V_o$ for Q_o. The capacitance ratio is assumed to be $C_{SI}/C_{PR} = 1$.

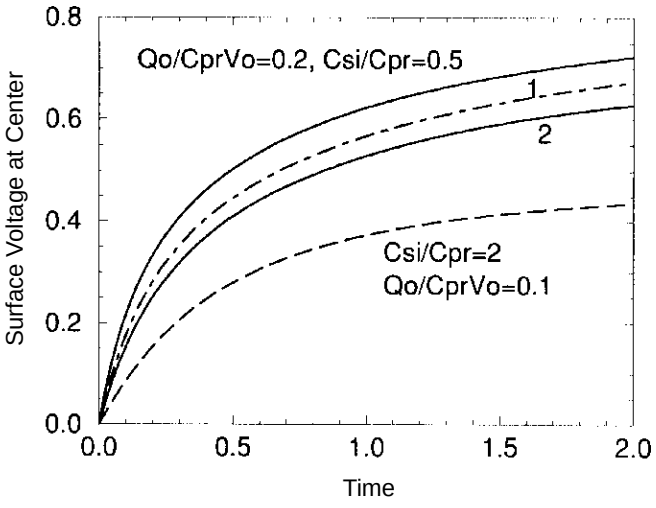

Figure 7. Calculated surface voltage at beam center as a function of time. For the three upper curves, the layer capacitance ratio C_{SI}/C_{PR} is varied with a fixed charge density. The Q_o and C_{SI}/C_{PR} values for the dashed and the dot-dashed curves are chosen so that the volume charge densities are the same. The units are t_o for time, V_o for voltage, and $C_{PR}V_o$ for Q_o.

extents of voltage recovery, or the image blurring, are the same for both cases.

If the PR capacitance is C_{PR} = 100 pF/cm, the unit of charge density is $C_{PR}V_o = 5 \times 10^{-8}$ Coul/cm^2, and the equilibrium charge density used in the above example is $Q_o = 0.2C_{PR}V_o = 10^{-8}$ Coul/cm^2. This corresponds to a sheet conductivity of $\Sigma = 2\mu Q_o = 10^{-13}$ S per square, with the above assumed μ value.

The dependence of the effect on the equilibrium charge density, Q_o (or the sheet conductivity Σ) is illustrated in Fig. 6. In this figure, the surface voltage at the beam center, $V(0,t)$, is plotted as a function of time after exposure for various values of Q_o. The unexposed surface voltage V_o and the ratio $C_{SI}/C_{PR} = 1$ are common to all curves. The recovery of surface voltage is seen to reach saturation in about one to two time units t_o, which can be a few milliseconds to a few tens of seconds depending on the beam size, as explained above. The data also indicate that the saturation voltage increases significantly as Q_o increases above $0.01(C_{PR}V_o)$, and it is less than 10% for lower Q_o. With the above typical values, the borderline value of $Q_o = 0.01$ $(C_{PR}V_o) = 0.5 \times 10^{-9}$ Coul/cm^2 corresponds to a sheet conductivity of $\Sigma \approx 0.5 \times 10^{-14}$ S per square, with the μ value used above.

In a similar plot of the beam center voltage versus time, shown in Fig. 7, the layer capacitance ratio C_{SI}/C_{PR} is varied. The Q_o value is chosen in the range where the effect is quite significant (i.e., $Q_o = 0.2C_{PR}V_o$). For a given Q_o (or sheet conductivity) the effect is seen to increase slightly with the decrease in the SI layer capacitance, which can result from the increase in the SI layer thickness L_{SI}. The deleterious effect of large L_{SI} is more significant when the results for the same volume charge density Q_o/L_{SI} are compared. For example, if the permittivities are the same, the dot-dashed curve (with $Q_o = 0.2$ and $C_{SI} = 1$) and the dashed curve (with $Q_o = 0.1$ and $C_{SI} = 2$) have the same volume charge densities. It can be seen that a factor of 2 larger thickness leads to a significantly larger voltage recovery and, hence, to a larger loss of voltage contrast.

The data in Figs. 6 and 7 also demonstrate that the two components of conductivity, namely, the charge density and the mobility, control the voltage recovery independently. In these plots, the charge mobility μ is implicit in the time units t_o, Eq. 7, which is proportionally smaller for a larger mobility. If the recoveries were uniquely determined by the μQ_o product–conductivity, then the same recovery for a smaller charge density (and a larger mobility) sample would be seen at a proportionally longer time. For example, in Fig. 6, if there were such a reciprocity between the density and mobility, the curve for a charge density of $Q_o = 0.03$ should coincide with that for $Q_o = 0.3$ when the time scale for the former is expanded by a factor of 10, (i.e., the data at t = 1 and 2 are plotted at t = 0.1 and 0.2, respectively). Also, extrapolating the former curve to t = 20, it is unlikely that the recovery would reach the corresponding value $V = 0.74$ for $Q_o = 0.3$ at t = 2. Such a failure of reciprocity between the density and mobility can also be seen in other sets of data.

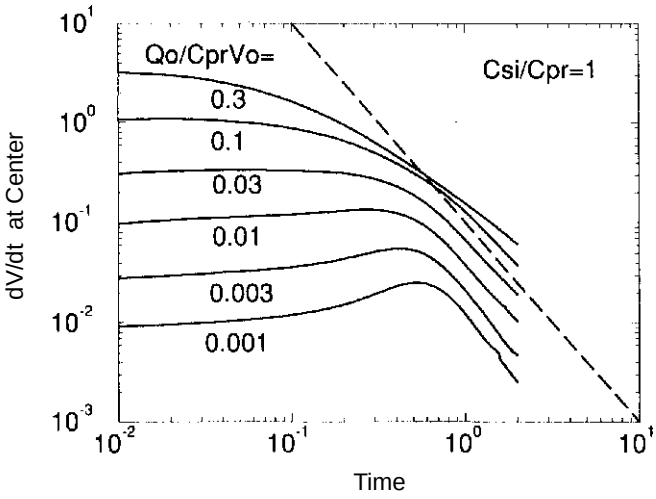

Figure 8. Time derivatives of calculated surface voltage at beam center (shown in Fig. 6), as function of time. The dashed line represents t^{-2} dependence.

The nature of charge conduction leading to this voltage recovery can be further illuminated by examining the time derivatives of the voltage, $dV(0,t)/dt$. Figure 8 shows the time derivatives of the voltage curves of Fig. 6 as functions of time. The derivative has a nearly constant value at short times and then decays at longer times, approximately after

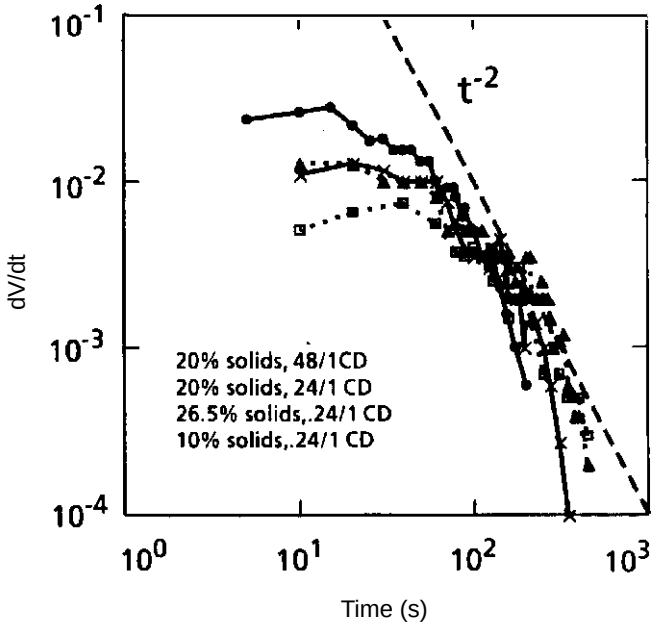

Figure 9. Time derivatives of experimental surface voltage as a function of time, for samples with various solid contents and charge director concentrations. The dashed line represents t^{-2} dependence.

$t > t_o$, according to the power law, t^{-n}, where $n \approx 2$. This is similar to the well-known characteristics of space-charge-limited transport,[13] associated with the decreasing of the driving field with time. Examples of the time derivatives of experimental recovery curves shown in Fig. 9 are in reasonable agreement with the t^{-2} law.

Conclusions

Considering the complexities associated with the experiments, such as the finite size of the probe, the finite time after exposure required for the discharge, the assumption of equal mobility for the positive and negative charges, and the neglect of dark decay in the PR, the agreement between the experimental results and the theoretical prediction is quite satisfactory.

In the previous theoretical models of lateral conduction,[1,3] the electrical properties of the SI layer were characterized by the sheet conductivity (or sheet resistance). This approach implicitly assumes the charge transport to be ohmic. In contrast, in the present theoretical analysis, the two components of conductivity, namely, the charge density and the mobility, are explicitly and independently considered in the transport equations. This method allows the roles of the two quantities to be clarified. The density determines the extent of voltage recovery (or image blurring), and the mobility determines the time required for the recovery (or blurring). The reciprocity between the density and mobility does not hold. Thus, for the SI layer not to cause any image blurring in time and extent of practical applications, not only the conductivity, but both its charge density and charge mobility, must be specified.

In summary, the theoretical analysis in a normalized units system enables results, obtained with relatively simple macroscopic experiments, to be used to predict the impact of the phenomenon in any high-resolution, high-speed regime of technological importance.

Acknowledgments. The authors are indebted to many of their colleagues: F. Bonsignore for the supply of liquid toners, S. Chang and C. Thornton for technical assistance in the preparation of concentrated toner layers, W. Wayman for instrumentation, and H. Till and R. Stover for helpful discussions.

References

1. T. Miyasaka, T. Umeda, T. Nagata, T. Igawa, and Y. Hori, Study of photoconductor resolutions by static latent images measurements, *J. Jap. Electrophotographic Soc.*, **30**: 432 (1991), also in *Proceedings of Japan Hardcopy '91*, p. 161 (1991).
2. E. J. Yarmchuk and G. E. Keefe, High-resolution surface charge measurements on an organic photoconductor, *J. Appl. Phys.* **66**: 5435 (19??); ibid., Motion of surface charge on layered organic photoconductor, *J. Imaging Sci.* **35**: 231 (1991).
3. D. S. Weiss, J. R. Cowdery, W. T. Ferrar, and R. H. Young, Analysis of electrostatic latent image blurring caused by photoreceptor surface treatment, *Proceedings of IS&T's 11th International Congress on Advances in Non-Impact Printing Technologies* p. 57, (1995).
4. J. Mort, F. Jansen, S. Grammatica, M. Morgan, and I. Chen, Field-effect phenomena in hydrogenated amorphous silicon photoreceptors, *J. Appl. Phys.* **55**: 3197 (1984); I. Chen, J. Mort, F. Jansen, S. Grammatica, and M. Morgan, Nature of electrophotographic images from amorphous silicon photoreceptors, *J. Imaging Sci.* **29**: 73 (1985).
5. S. Yagi, M. Nishikawa, and K. Karakida, Field effect in SiN_x-overcoated amorphous silicon photoreceptors observed by xerographic discharge method, *J. Non-Cryst. Solids* **115**: 210 (1989).
6. (a) H. Yamamoto, Y. Takashima, H. Terada, H. Kunishige, and T. Saitoh, Novel color electrophotography: one drum color-superimposing process, *Paper Summaries, SPSE's 5th International Congress on Advances in Non-Impact Printing Technologies,* p. 65 (1989); (b) Ibid., Novel color electrophotography by one drum color superimposing process, *J. Jap. Electrophotographic Soc.* **28**: 284 (1989); (c) Ibid., One drum color superimposing process, *J. Jap. Electrophotographic Soc.* **29**: 9 and 14, (1990).
7. H. Yamamoto, Electrostatic effects of the toner layer on the photoconductor, *Paper Summaries of SPSE's 6th International Congress on Advances in Non-Impact Printing Technologies*, p. 17 (1990).
8. I. Chen, Developability of interposed imagewise charge in color electrophotography, *J. Imaging Sci.* **35**: 365 (1991).
9. B. Landa, Y. Niv, Y. Almog, and P. Ben Avraham, A comparison of Electroink™ and conventional liquid toner *Paper Summaries, SPSE's 5th International Congress on Advances in Non-Impact Printing Technologies*, p. 203 (1989).
10. For general information about liquid toners see S. P. Schmidt, J. R. Larson, and R. Bhattacharya, Liquid toner technology, in *The Handbook of Imaging Materials* A. Diamond, Ed., Marcel Dekker, New York, 1991.
11. For recent work on charge director micelle ionization see J. R. Larson, I. D. Morrison, and T. S. Robinson, A thermodynamic approach to liquid toner particle charging and charge director ionization, *Proceedings of IS&T's 8th International Congress on Advances in Non-Impact Printing Technologies*, p. 193 (1992).
12. The liquid toners used are very similar to those described in Ref. 11, except in this case the charge directors used are ammonium block copolymers. For further information about these materials see L. A. Page and L. M. El-Sayed, AB diblock copolymers as charge directors in liquid toners, *Hardcopy and Printing Materials, Media and Processes, Proc. SPIE*, **1253**: p. 37 (1990) and J. R. Larson, J. W. Spiewak, J. Mort, I. Chen, M. Abkowitz, and H. Antoniadis, Liquid developer compositions with block copolymers, US Patent 5,459,007 (October 17, 1995).
13. I. Chen, Xerographic discharge characteristics of photoreceptors II, *J. Appl. Phys.* **43**: 1137 (1972); J. Mort and I. Chen, Physics of xerographic photoreceptors, in *Applied Solid State Science*, R. Wolfe, Ed., Academic Press, New York, 1975, Vol. **5**, p. 69.